Automatic Intrinsic Calibration of Double-sided Silicon Strip Detectors

Reese, M.; Gerl, J.; Golubev, Pavel; Pietralla, N.

Published in:
Nuclear Instruments & Methods in Physics Research. Section A: Accelerators, Spectrometers, Detectors, and Associated Equipment

DOI:
10.1016/j.nima.2015.01.032

2015

Automatic Intrinsic Calibration of Double-Sided Silicon Strip Detectors

M. Reese[a,*], J. Gerl[b], P. Golubev[c], N. Pietralla[a]

[a] *Institut für Kernphysik, Technische Universität Darmstadt, 64289 Darmstadt, Germany*
[b] *GSI Helmholtzzentrum fr Schwerionenforschung GmbH, 64291 Darmstadt, Germany*
[c] *Department of Physics, Lund University, SE-22100 Lund, Sweden*

Abstract

A reliable and simple-to-use algorithm was developed for the energy-calibration of double-sided silicon strip detectors (DSSSD). It works by enforcing mutual consistency of p-side and n-side information for every detected event. The procedure does not rely on a dedicated data set for calibration and is robust enough to work fully automated without human supervision. The method was developed and applied to data from a DSSSD of the Lund-York-Cologne CAlorimeter (LYCCA) for the HISPEC experiment at FAIR. It has been tested on ions in the $A \approx 90$ mass range at energies of $E_{\mathrm{kin}} \approx 300$ MeV/u.

Keywords: calibration procedure, silicon strip detector, energy loss measurement

1. Introduction

Double-sided silicon strip detectors (DSSSD) are widely used for charged particle detection in nuclear and particle physics experiments to obtain position, energy or energy-loss information and particle identification [1]. They are constructed as large area silicon detectors with segmented p-side and n-side contacts. The intersecting areas of both side's segments form pixels. All signals on both sides are read out through individual channels. For each event, the channel numbers on both sides indicate the pixel that was hit by the charged particle.

*Corresponding author
Email address: reese@ikp.tu-darmstadt.de (M. Reese)

Typical applications for DSSSDs make use of square [1] or circular shapes [2] (see Fig. 1). In applications where energy information is required, it is essen-

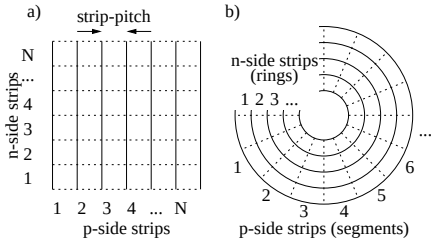

Figure 1: Schematic view of two common configurations for DSSSDs: a) shows a rectangular shaped, b) a circular shaped segmentation layout. Solid and dashed lines indicate the borders of front-side and back-side segments, respectively.

tial to calibrate the individual segments of the DSSSD. We distinguish between "absolute" and "intrinsic" calibration of such detectors in the following way: By "absolute energy calibration", we refer to a set of calibration coefficients that map measured amplitudes to units of energy. A set of coefficients can be obtained by recording spectra for all segments using particle sources of known energy, such as α-sources, or a particle beam from an accelerator. By analyzing these spectra, single segment gains can be obtained in units of energy per ADC-channel. In addition, pulsers can be used to inject charge with calibrated value into the front end electronics (FEE)[1] of all strips [2], to correct for non-linearities in the FEE. For highly segmented DSSSDs, this procedure is difficult for two reasons: First, the analysis has to be performed for each channel, i.e. the effort increases with the number of channels. Second, and more important, the active area per segment decreases with higher segmentation. Consequently, a long measurement time for calibration is required to accumulate a sufficient number of events in the calibration spectra. This can be exceedingly expensive if an accelerator is used as a calibration source.

An absolute calibration implies that all segments deliver comparable infor-

[1] only the FEE, not the detector itself is calibrated by this method

mation about the energy-loss of a particle, i.e. the information doesn't depend on which strip was hit. If this is the case, but the absolute energy scale is not determined, we call this "intrinsic calibration". Intrinsic calibration of the individual strips of the detector is sufficient, for example in particle tracking and identification applications [1, 3].

A detector with pre-existing intrinsic calibration of the individual strips is easier to calibrate absolutely with known sources. The problem of increasing measurement time for highly segmented detectors does not occur, because the segmentation does not matter anymore, as far as the calibration spectrum is concerned.

In this work we will show that it is possible to obtain an intrinsic calibration for DSSSDs by using the correlations of p-side and n-side data. We demonstrate this by presenting one possible algorithm that exploits these correlations to obtain a set of intrinsic calibration coefficients from any data set from the detector. Further, we show results of its application to data from a DSSSD, that was used as part of the Lund-York-Cologne-Calorimeter (LYCCA), a detector system for relativistic heavy-ion identification and tracking. Finally, limitations and possible improvements of the method will be discussed.

2. Method

For a single event of energy deposition inside a DSSSD, the created charge carriers induce signals in all electrical segments as they move within the detector volume. The measured signal amplitudes depend on the geometry of the detector and it's segmentation, in particular, of the distance between the segment and the location of charge carriers. Cross-talk between different channels in the FEE can modify the signal amplitudes of all channels. The presented algorithm neglects cross-talk in the FEE and assumes that there is at least a fraction of events, where the deposited energy

$$E = s_i \, A_i \, , \tag{1}$$

in the detector is proportional to a signal in channel i of amplitude A_i, and that all other channel amplitudes are negligible:

$$A_i \gg A_j \quad \text{for} \quad i \neq j\,. \tag{2}$$

The slope factor s_i is the only calibration coefficient for a given channel i. In section 4 we will generalize (1), allowing for an additional offset in the energy dependence. Note, that the principle of correlating p-side and n-side information does not demand the exclusion of cross-talk and multi-segment hits. However, this simplified treatment turned out to be sufficient for achieving good results as will be shown in Section 5.

The basic idea of the procedure is the following: Given a DSSSD with N_p and N_n strips on the p-side and n-side, respectively, each event that is registered in a given pixel will create a signal with amplitude A_p in the strip number p on the p-side and a signal with amplitude A_n in strip number n on the n-side $(n, p = 1 \ldots N_{n,p})$. Assuming that both strips measure the same deposited energy E in the active area of the detector, one can write

$$E_p = s_p\, A_p\,, \quad E_n = s_n\, A_n \quad \text{and} \quad E_p = E_n = E\,, \tag{3}$$

with s_p and s_n being the calibration coefficients (slopes) for the p-th p-side strip and the n-th n-side strip, respectively. For each pixel that was hit, the corresponding segments on both sides will deliver signal amplitudes, A_p and A_n, that are unambiguously related. Since we assume in this section that Eq. (1) is valid, this relation between the two measured amplitudes is also linear without offset

$$A_p = S_{pn}\, A_n\,. \tag{4}$$

The slope $S_{pn} = A_p/A_n$ of this line can be experimentally determined for each pixel, based on a given set of measured events. A schematic representation of the relations can be seen in Fig. 2. For each pixel, this slope can be visualized by plotting for each event the amplitudes (A_p and A_n). Fig. 3 shows such a plot for measured data of a single DSSSD pixel, which allows to determine S_{pn} and it's uncertainty ΔS_{pn} for this pixel. The set of $N_p\, N_n$ measured S_{pn}-values

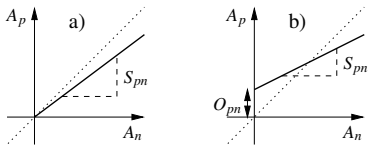

Figure 2: The relation between A_p and A_n for one single pixel of the detector (thick, solid line) with slope S_{pn}. In general, this line does not coincide with the diagonal (dotted line). In a) no offset is present, while in b) an offset O_{pn} is allowed (see section 4).

can be used to get a set of $N_p + N_n$ calibration coefficients $\{s_p, s_n\}$ that best reproduces the set of measured $\{S_{pn}\}$. Both sets are related by

$$S_{pn} = \frac{s_n}{s_p}\,, \tag{5}$$

which follows from Eqs. (3,4). One way of finding a set of $2\,N$ calibration parameters $\{s_p, s_n\}$ is to minimize the following expression

$$\chi^2 = \sum_{p,n} \left(\frac{S_{pn} - \frac{s_n}{s_p}}{\Delta S_{pn}} \right)^2 , \tag{6}$$

where ΔS_{pn} is the experimental uncertainty for the pixel slopes S_{pn}. The calibration parameters that minimize (6), also fulfill the condition (3) and therefore represent the best set of calibration coefficients for a given input data set on an arbitrary scale, if the simplifying assumptions are valid.

The proposed method, as described above, requires the following conditions to be fulfilled: It is essential, that p-side and n-side strips have intersection points and that both side's strips are read-out. In addition, a sufficient amount of single-strip events has to be present, i.e. events where (2) is valid. Events with inter-strip hits on one or both sides will contribute to the background and should be excluded from the calibration procedure. Note, that this procedure could also be applied to detectors with segmentation on one side only, as long as signals from all segments and the un-segmented side are recorded.

3. Implementation

The presented implementation uses two essentially independent steps: First, the determination of S_{pn} and the uncertainty ΔS_{pn} for each pixel from measured

data. Second, the calculation of a set of calibration coefficients $\{s_p, s_n\}$ based on the set of $\{S_{pn}, \Delta S_{pn}\}$ from the first step. The former is done using a Bayesian [4] approach, and the latter is done by using a nonlinear least squares fit algorithm. Both steps are described in the following two subsections.

3.1. Determination of S_{pn}

For all pixels, the slope coefficient $S_{pn} = A_p/A_n$ is computed from the data obtained from M selected events in the detector, each event consisting of two amplitude measurements $A_{p,i}, A_{n,i}$ that obey (2). An obvious way to determine S_{pn}, would be a straight line fit to the 2d-distribution of all amplitude pairs using a χ^2 minimization procedure, as illustrated in Fig. 3. The slope of that line would correspond to S_{pn}. Doing so, the resulting S_{pn} has a systematic

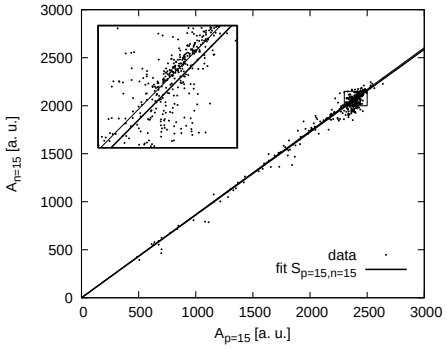

Figure 3: This plot shows a typical distribution p/n-side amplitude pairs (dots) for a single pixel (p=15, n=15), after selecting single-strip events on both sides as described in section 2. Even though there is not much background, a simple χ^2-fit (thick, solid line) of the slope S_{pn} misses the correct value. The inset shows a zoom-in to the most densely populated part of the graph where the mismatch of data and χ^2-fit is obvious to the human eye. For comparison, the thin solid line shows the result determined by our algorithm.

error, as can be seen in the inset of Fig. 3. This is because the χ^2 minimization procedure assumes a Gaussian distribution of the individual points around the fitted function, and the result can be significantly changed if some points violate this assumption. There are several suggestions in [4] to overcome this problem. One approach is to assume distributions with outreaching tails for data points

around the fitted function, such as the Cauchy-Lorentz distribution. This weakens the impact of few outliers in the data. Instead of implementing such a fitting routine and apply it to the input data, it is possible to compute a probability distribution for the quantity of interest directly, by repeated usage of Bayes' theorem (7). This is simple to implement because it requires for each event, a point-by-point multiplication of two functions, namely the distribution based on all previous events and the likelihood function of the current event. After multiplication, a normalization step follows to qualify the result as probability distribution. The details are described in the following:

Our goal is the computation of the posterior probability distribution $p\,(\,S_{pn}|\,\{A_p, A_n\}_M)$ of the quantity of interest S_{pn} for all pixels of the detector. The notation was adopted from [4], where $p(x|y)\,dx$ is a function of the variable x that gives the probability of having x in the interval $[x, x+dx]$ if some condition (or information) y is given. We define the subset $\{A_p, A_n\}_i := \{A_{p,1}, A_{n,1}, A_{p,2}, A_{n,2}, \ldots, A_{p,i}, A_{n,i}\}$ as the data obtained from the first i measured events. Obviously, $\{A_p, A_n\}_M$ is the set of all measured events. The most likely value for the slope parameter S_{pn} and its error ΔS_{pn} for each p and n can be obtained from the mean and variance of the final posterior distribution. Calculating $p\,(\,S_{pn}|\,\{A_p, A_n\}_M)$ is done iteratively, treating one event after the other, while the width of the distribution becomes narrower with each step. The iteration starts with an initial guess for the $p_0\,(S_{pn})$ distribution, in this case uniform within reasonable limits $S_{\min}$ and $S_{\max}$. These limits should cover all occurring values of S_{pn}, which can be estimated by the maximum expected ratio of gains in all channels: $S_{\min} < \min(s_n/s_p)$ and $S_{\max} > \max(s_n/s_p)$. For example, if the smallest gain is expected to be no less than 10 times the largest gain, S_{pn} can be inside the interval $[0.1, 10]$. For each event, $p_0\,(S_{pn})$ is refined by applying Bayes' theorem [4, 5, 6]

$$p_i\,(S_{pn}\,|\{A_p, A_n\}_i\,) = \frac{p_i\,(S_{pn})\;L\,(\,A_{p,i}, A_{n,i}|\,S_{pn})}{p\,(A_{p,i}, A_{n,i})}\,, \tag{7}$$

with the commonly used terminology [4]: $p_i\,(S_{pn}\,|\{A_p, A_n\}_i\,)$ is called *posterior* distribution, $p_i\,(S_{pn})$ is the *prior* distribution, $L\,(\,A_{p,i}, A_{n,i}|\,S_{pn})$ the *likelihood*

function and $p\left(A_{p,i}, A_{n,i}\right)$ is a normalization factor that is also called *evidence* of the measured data. Index i indicates the iteration step. After each event, the normalized posterior distribution becomes the prior for the next data point

$$p_{i+1}\left(S_{pn}\right) = p_i\left(S_{pn}\,|\{A_p, A_n\}_i\right) , \tag{8}$$

and the final distribution is obtained at the last iteration. The likelihood function is chosen to be a Cauchy-Lorentz distribution with width w

$$L\left(A_{p,i}, A_{n,i}|\, S_{pn}\right) \propto \frac{1}{w^2 + \left(\log \frac{A_{p,i}}{A_{n,i}} - \log S_{pn}\right)^2} . \tag{9}$$

This particular choice for the likelihood function was inspired by the aforementioned treatment of fitting data with outliers in [4]. Other distributions were not tested, because satisfactory results were obtained.

According to the central limit theorem, the posterior distribution approaches a Gaussian shape. However, no analytic expression for the distribution at intermediate steps of the calculation is known. Thus, the posterior distribution has to be approximated by a discrete number K of points between $S_{\min}$ and $S_{\max}$. The value of K depends on the chosen limits $S_{\min,\max}$ and the desired accuracy of the final result. Typical values are in the order of a few thousand.

3.2. Computing a set of calibration coefficients

Minimization of (6) is done using the implementation of a standard nonlinear least squares fit provided by the GNU Scientific Library [7]. The set of fit parameters is $\{s_p, s_n\}$, and the input data is the complete set of measured parameters $\{S_{pn}\}$. To allow for a unique solution, one out of the $N_p + N_n$ parameters has to be fixed, for example by setting one of the p-side slopes to 1. The algorithm attempts to minimize Eq. (6) with respect to the remaining $N_p + N_n - 1$ parameters. After convergence is reached, the resulting parameter set describes the best intrinsic calibration coefficients for the individual strips relative to each other on a common arbitrary scale. The algorithm works automatically in the following sense: Once a good parameter set $(K, S_{\min}, S_{\max}, w)$

is found for a detector, intrinsic calibration coefficients can be found for it by analyzing any measured data set.

4. Offset determination

For cases in which the offsets are not negligible, the method can be extended to take them into account. This was done in the following way: An offset o is added to Eq. (1)

$$E = o + s\,A\,. \tag{10}$$

If offsets are allowed, the linear dependence between A_p and A_n is also allowed to have an offset O_{pn}. This changes Eq. (4) into (see Fig.2 b)

$$A_p = O_{pn} + S_{pn}\,A_n\,. \tag{11}$$

The first step, determination of O_{pn} and S_{pn}, can be achieved with two-dimensional probability density functions $p\,(S_{pn}, O_{pn}|\,\{A_p, A_n\})$. The basic procedure is the same as described in 3.1. Only the likelihood function has to be extended from (9) to be two-dimensional, taking into account the correlation between offset and slope:

$$L\,(\,A_{p,i}, A_{n,i}|\,S_{pn}, O_{pn}) \propto \frac{1}{w^2 + \left(\log \frac{A_{p,i}-O_{pn}}{A_{n,i}} - \log S_{pn}\right)^2}\,. \tag{12}$$

For the numerical approximation, a range of possible offset parameters O_{pn} has to be specified by two additional parameters, $O_{\min}$ and $O_{\max}$. These limits have to be chosen such, that they include all occurring O_{pn} as defined in (13). The numerical approximation of the two-dimensional posterior distribution in a computer requires significantly more memory and computation time than in the one-dimensional case, but it is possible on nowadays desktop computers.

The second step, calculation of the coefficients for each strip, has to be modified as well. All relevant quantities are related as in Eq. (5), but with an additional equation for the offset:

$$S_{pn} = \frac{s_n}{s_p} \quad \text{and} \quad O_{pn} = \frac{o_n - o_p}{s_p}. \tag{13}$$

With the modified relations of Eq. (13), the set of $2\,N_p + 2\,N_n - 2$ calibration parameters $\{o_p, s_p, o_n, s_n\}$ can be found by minimizing Eq. (14), which is an extended form of Eq. (6):

$$\chi^2 = \sum_{p,n} \left(\frac{S_{pn} - \frac{s_n}{s_p}}{\Delta S_{pn}} \right)^2 + \left(\frac{O_{pn} - \frac{o_n - o_p}{s_p}}{\Delta O_{pn}} \right)^2 . \tag{14}$$

where S_{pn}, O_{pn} and $\Delta S_{pn}, \Delta O_{pn}$ are mean and variance of the final distribution $p\left(S_{pn}, O_{pn} | \{A_p, A_n\}\right)$. Again, two parameters have to be fixed to find a unique solution, for example $o_N = 0$ and $s_N = 1$.

5. Experimental Data

The method was developed and tested, using data from one of the DSSSDs of LYCCA [1], which is part of the PreSPEC-AGATA setup [8] at the GSI Helmholtzzentrum for Heavy Ion Research. Results shown here are based on data from the PreSPEC-AGATA campaign in 2012. During that campaign, LYCCA contained 17 DSSSD modules, each being 300 μm thick. We present data for the DSSSD close to the position of the secondary target with 32 strips on both sides. The strip pitch is 1.8 mm, with an inter-strip isolation of 30 μm. A schematic block diagram of the read-out chain is shown in Fig. 4. More details about the FEE are described in [1]. A primary beam of ^{86}Kr

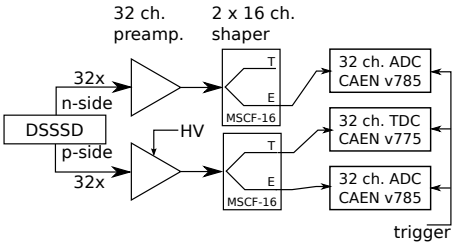

Figure 4: Custom made preamplifiers [1] are used to provide differential input signal for the commercially available MSCF-16. These modules contain sixteen channel shaping amplifiers and timing filter amplifiers with leading edge discriminators. The MSCF-16 output is recorded by two CAENv758 ADC and a CAENv757 TDC inside a VME crate that is part of the PreSPEC MBS data-acquisition system.

was accelerated with the GSI Universal Linear Accelerator (UNILAC) and the SchwerIonen Synchrotron (SIS18). A mixture of different nuclear species was created by the collision of the primary beam with a thick beryllium target. The GSI Fragment Separator (FRS) [9] was tuned to select an almost pure beam of ^{85}Br ions with kinetic energies of about 306 MeV/u when entering the DSSSD. Under these conditions about 255 MeV are deposited inside the DSSSD, according to a calculation with the computer program LISE++ [10].

6. Results

In the following all, presented data is after selecting single strip events according to (2). Fig. 5 shows the amplitude of the n-side plotted versus the

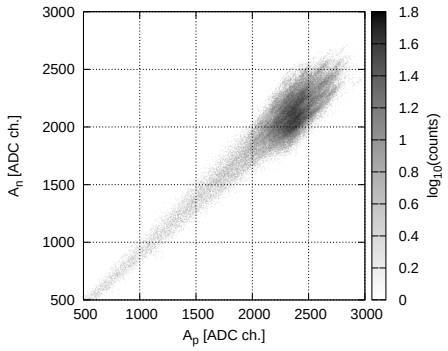

Figure 5: Shown is an overlay histogram of n-side amplitude A_n vs p-side amplitude A_p for all possible pairings of n and p. The broad structure can be interpreted as an overlay of all lines with slopes S_{pn}. After applying the calibration procedure, the picture changes to Fig. 6.

amplitude of the p-side, for events with strip multiplicity one on both sides. The histogram is the sum of all pixels of the detector. Without calibration, the p-side and n-side amplitudes are in general different from each other, resulting in a broad structure around the $A_n = A_p$ diagonal. After applying the calibration procedure described in this work, the outputs of all pixels are aligned. This is verified by Fig. 6, where the amplitudes were multiplied with their respective gain-match factors s_p and s_n. The parameters for the algo-

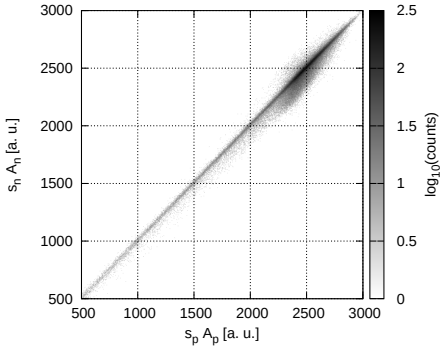

Figure 6: Overlay histogram of calibrated n-side amplitude $s_n\,A_n$ vs calibrated p-side Amplitude $s_p\,A_p$ for all possible pairings of n and p. Calibration factors s_n and s_p were determined using the method described in this work. Obviously, p- and n-side energy measurements are in agreement, regardless of which pair of strips is hit.

rithm were for the no-offset version $5000, 0.6, 1.4, 0.01$ for $K, S_{\min}, S_{\max}$ and w, respectively. For the algorithm with offset determination, the parameter set was $800, 0.6, 1.4, 0.01, 200, -200, 200$ for $K_s, S_{\min}, S_{\max}$, w, $K_o, O_{\min}$ and $O_{\max}$, respectively.

In order to quantify the relative resolution of the detector at different amplitudes, the disagreement between calibrated p-side and n-side amplitudes $s_p\,A_p - s_n\,A_n$ is plotted over the calibrated p-side amplitude $s_p\,A_p$ in Fig. 7. This plot contains essentially the same information as 6, but the diagonal is transformed onto the $s_p\,A_p$-axis, and allows for determination of the width of the distribution by projecting to the other axis. If no offsets are determined, the resulting calibration will have the best resolution at the most intense part of the energy spectrum, where most of the recorded events are situated. The resolution gets worse for events where the amplitude differs significantly from the peak in the spectrum. This effect is highlighted in Fig. 8, where the achieved resolution for different regions of the amplitude spectrum is shown. If the full range of the spectrum is of relevance, offsets shouldn't be neglected. In the lower parts of the spectrum with less intensity, the resolution of the slope-only calibration is significantly worse than the one including offsets.

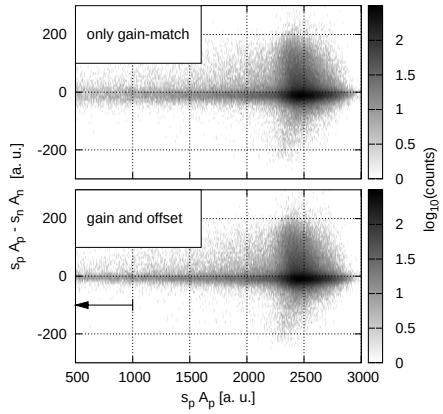

Figure 7: Both histograms show the difference of the calibrated amplitude of p-side and n-side, plotted over the calibrated p-side amplitude (similar information as Fig. 6). In the upper picture, the calibration procedure was applied without determining offsets. The lower picture shows the improvement after the calibration of both, offsets and gains. Differences are predominantly apparent for events with lower amplitudes (indicated by the arrow), where the missing offsets have a significant impact. This can be seen even better in Fig. 8.

The peaks in Fig. 8 can be used to estimate the relative resolution of the detector. The width (FWHM) of that peak amounts to $\Delta = 27.4$ a.u.. Assuming that both sides measure the same energy independently with approximately the same accuracy, i.e. $\sigma_p \approx \sigma_n \approx \sigma$, the difference of the measurements of both sides will have a width of $\Delta = \sqrt{\sigma_p^2 + \sigma_n^2} \approx \sqrt{2}\,\sigma$. If both, p and n-side measurement are combined to form an average, the uncertainty of the measured energy deposition can be approximated with $\sigma/\sqrt{2} = \Delta/2$. The peak width Δ is dominated by events with an amplitude of around 2400 a.u. (see Fig. 6), which corresponds to the energy loss of the ^{85}Br particles. Thus, the relative resolution in the most relevant region of the spectrum corresponds to 0.57 % at 255 MeV, which is well within the expected range between 0.5 % and 1 %, as stated in [1]. This indicates, that the calibration method works correctly. Note, that the method was tested for fast particles, where none of them is stopped inside the detector material. Since the only assumption is the agreement of n-side and p-side charge collection, it should work as well for lower energies when particles are implanted.

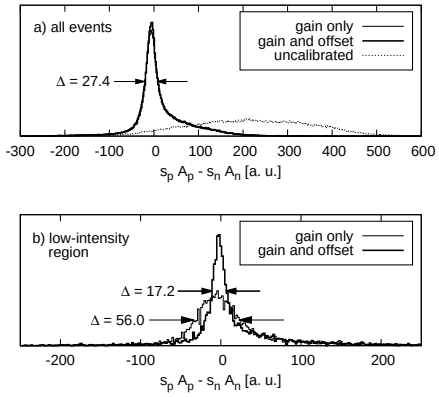

Figure 8: a) The difference of calibrated p-side and n-side amplitude for all amplitudes. b) The same quantity for amplitudes below a value of 1000 as indicated by the arrow in Fig 7. Δ indicates the full with at half maximum of the peaks.

7. Possible Improvements

In the procedure described here, the user has to fix the parameters for the range of the probability distributions and their density of points. If the range is not known, the user has to choose a wide and fine enough grid for the representation of the distribution and pays with longer computation time and more memory consumption. Especially in the case of two-dimensional distributions for gain and offset determination, this can reach the limits of the available hardware in a common desktop computer. Therefore, it would be a significant improvement in performance and usability, if the probability distributions would be adaptive in range and density of points. If such an improvement would be implemented, the only remaining parameter would be the width w of the likelihood function in Eqs. (9,12).

For the calibration with offsets, there is a strong negative correlation between the measured quantities S_{pn} and O_{pn}. This could be taken into account by minimizing, instead of Eq. (14), the expression

$$\chi^2_{\mathrm{cor}} = \sum_{p,n} \left(S_{pn} - \frac{s_n}{s_p}, O_{pn} - \frac{o_n - o_p}{s_p} \right) \mathrm{Cov}^{-1}_{pn} \left(S_{pn} - \frac{s_n}{s_p} O_{pn} - \frac{o_n - o_p}{s_p} \right) . \tag{15}$$

with Cov_{pn}^{-1} the inverse of the covariance matrix of the posterior probability distribution $p(S_{pn}|\{A_p, A_n\}_M)$. This should improve the precision of the calibration coefficients for the same amount of data.

8. Summary

A reliable method for the intrinsic calibration of DSSSD strips among each other was developed, implemented and tested with in-beam production data. The main advantage over conventional calibration procedures is the ability to work with any data set with any kind of energy distribution. If an absolute energy calibration of the detector is needed, the method can still be of considerable use if it is applied before the absolute calibration, in which case the detector can be treated as one device instead of a collection of independent strips. Possible future improvements of the implementation have been suggested.

9. Acknowledgments

This work is supported by the German Federal Ministry for Education and Research under grant No. 05P12RDFN8 (TP6), NuSTAR.De, and by the LOEWE program of the State of Hesse within the Helmholtz International Center for FAIR (HIC for FAIR).

References

[1] P. Golubev, et al., Nucl. Instr. and Meth. A 723 (2013) 55.

[2] A. Ostrowski, et al., Nucl. Instr. and Meth. A 480 (2002) 448.

[3] R. Kumar, et al., Nucl. Instr. and Meth. A 598 (2009) 754.

[4] D. S. Sivia, Data Analysis: A Bayesian Tutorial, 2nd Edition, Oxford Univ. Press, 2006.

[5] T. Bayes, Philosophical Transactions 53 (1763) 269.

[6] P. S. Laplace, Statistical Science 1 (1986) 364.

[7] B. Gough, GNU Scientific Library Reference Manual - Third Edition, 3rd Edition, Network Theory Ltd., 2009.

[8] N. Pietralla, et al., EPJ Web of Conferences 66 (2014) 02083.

[9] H. Geissel, et al., Nucl. Instr. and Meth. B 70 (1992) 286.

[10] O. Tarasov, et al., Nucl. Instr. and Meth. B 266.